Liu *et al.*
Chinese Journal of Mechanical Engineering (2024) 37:73
https://doi.org/10.1186/s10033-024-01058-w

Chinese Journal of Mechanical Engineering

ORIGINAL ARTICLE

Open Access

Calculation and Analysis of TVMS Considering Profile Shifts and Surface Wear Evolution Process of Spur Gear

Wenzheng Liu[1], Rupeng Zhu[1*], Wenguang Zhou[1] and Jingjing Wang[1]

Abstract

Profile shift is a highly effective technique for optimizing the performance of spur gear transmission systems. However, tooth surface wear is inevitable during gear meshing due to inadequate lubrication and long-term operation. Both profile shift and tooth surface wear (TSW) can impact the meshing characteristics by altering the involute tooth profile. In this study, a tooth stiffness model of spur gears that incorporates profile shift, TSW, tooth deformation, tooth contact deformation, fillet-foundation deformation, and gear body structure coupling is established. This model efficiently and accurately determines the time-varying mesh stiffness (TVMS). Additionally, an improved wear depth prediction method for spur gears is developed, which takes into consideration the mutually prime teeth numbers and more accurately reflects actual gear meshing conditions. Results show that consideration of the mutual prime of teeth numbers will have a certain impact on the TSW process. Furthermore, the finite element method (FEM) is employed to accurately verify the values of TVMS and load sharing ratio (LSR) of profile-shifted gears and worn gears. This study quantitatively analyzes the effect of profile shift on the surface wear process, which suggests that gear profile shift can partially alleviate the negative effects of TSW. The contribution of this study provides valuable insights into the design and maintenance of spur gear systems.

Keywords Profile shift, Tooth surface wear, Structure coupling effect, Improved wear depth prediction method, TVMS

1 Introduction

Gears play a vital role in power and motion transmission for various applications, including helicopters, wind turbines, and other fields [1, 2]. Tooth surface wear is inevitable during operation, leading to deviations in the tooth profile due to material removed from the tooth surface [3]. In order to enhance gear performance, particularly under heavy loads, gear profile shift is often implemented [4], which involves altering the tooth profile of a gear. Both profile shift and tooth wear can impact the meshing characteristics by altering the involute tooth profile. Therefore, research that examines the effect of profile shift and wear processes is of great value.

According to previous studies, the variation of the tooth profile induced by surface wear can lead to changes in the load distribution across the tooth profile [5, 6]. Additionally, the profile shift of a spur gear can also influence the TVMS and LSR to improve the meshing characteristics [7, 8]. Consequently, the precise calculation of key parameters such as the TVMS and LSR for profile-shifted and worn gears is of great significance for this study. Chen et al. [5] presented an evolution of the influences of TSW on TVMS, which established a TVMS model to calculate the stiffness with different wear degrees. Huangfu et al. [6] simulated wear depth according to the FEM, and the proposed method can greatly reduce computation time. The mesh stiffness under different modification coefficients can be obtained in Ref [7], which indicates

*Correspondence:
Rupeng Zhu
rpzhu_nuaa@163.com
[1] College of Mechanical and Electrical Engineering, Nanjing University of Aeronautics and Astronautics, Nanjing, China

the influence of profile shift on TVMS. However, the tooth deflection due to the neighboring loaded tooth is not considered in these works [5–8]. In recent years, the deflection of the tooth caused by the structure coupling has been observed in some research [9–11]. Xie et al. [12] introduced the structure coupling effect in the fillet foundation stiffness calculation process. Furthermore, a comprehensive analytical gear mesh stiffness model considering tooth error was established by Chen et al. [13], which also includes the gear body structure coupling effect as well as tooth profile deviations. Recently, Chen et al. [14] built an improved model for TVMS considering tooth surface wear, and the TVMS and transmission error with tooth profile modification and wear fault have been analyzed. Nevertheless, a stiffness calculation model including profile shift, surface wear, tooth deformation, tooth contact deformation, fillet-foundation deformation, and gear body structure coupling effect has not been fully considered.

At present, many researchers have focused on the tooth surface wear process, which has a significant influence on meshing stiffness. Archard's wear model [15] has been widely used for calculations of wear depth [16–18]. Ding et al. [19] proposed a gear wear model that includes the influence of the worn profile to study the interaction of surface wear and dynamic behavior. Shen et al. [20] calculated the planetary gear wear depth according to Archard's equation and incorporated it into the dynamic model due to the TVMS. Feng et al. [21] put forward a new approach to calculate the wear depth distribution of gears; the wear model is improved with consideration of contact pressure, which is more reasonable. Wang et al. [22] developed a numerical model with high computational accuracy for elastic rough surface contact and predicted tooth surface wear for spur gears. Liu et al. [23] proposed a dynamic wear prediction methodology to investigate the coupling effects between surface wear and dynamics of spur gear systems. Besides, the calculation results by Archard's wear equation are mainly dependent on load distribution and lubrication condition [5]. Therefore, accurate calculation of key parameters such as the TVMS and LSR is essential since they are continuously updated during the meshing process.

In addition, the analysis and research on the influence between gear profile shift and tooth surface wear are still insufficient. There remains a lack of comprehensive investigation into the correlation and synergy between gear profile shift and tooth surface wear. Avil et al. [23] simulated wear on a combination of different tooth-sum alterations and profile shift factors based on a generalized Archard's wear equation. Zhou et al. [24] proposed a TVMS model of a modified gear–rack drive with tooth friction and wear, which presents the influence of the modification coefficient and pressure angle on the TVMS of the gear-rack drive. The performance of the gear–rack drive can be enhanced by optimizing the modification coefficient. Furthermore, selecting an appropriate modification coefficient may weaken the negative influence of tooth wear.

In this paper, a tooth stiffness model including profile shift, surface wear, tooth deformation, tooth contact deformation, fillet-foundation deformation, and gear body structure coupling has been established. Then, an improved wear depth prediction method for spur gears considering the mutual prime of teeth number is proposed. The values of TVMS and LSR of profile-shifted gears and worn gears are verified by FEM. Finally, the effect of profile shift on the wear process is discussed. The structure of this paper is shown in Figure 1.

The significance of this research lies in the establishment and accurate verification, through FEM, of a tooth stiffness model that incorporates profile shift, surface wear, tooth deformation, tooth contact deformation, fillet-foundation deformation, and gear body structure coupling. This calculation efficiency is greatly improved compared with FEM. Additionally, an improved wear prediction method has been developed, which takes into consideration the mutually prime teeth numbers and more accurately reflects actual gear meshing conditions. On the basis of quantitative analysis, this paper suggests that gear profile shift can partially alleviate the negative effects of TSW and thus can be a useful guide for design.

2 TVMS of the Profile-Shifted Spur Gear Considering TSW

2.1 Tooth Stiffness Model of Profile-shifted Spur Gear with TSW

In this section, a tooth stiffness model of profile-shifted gear with TSW is proposed. Compared with the standard involute gear, the tooth of the profile-shifted spur gear with TSW is regarded as a nonuniform cantilever beam model. From the perspective of potential energy theory [25, 26], the meshing stiffness is separated into Hertzian contact energy, bending energy, shear energy, axial compressive energy, and fillet-foundation energy.

The tooth deformation of the profile-shifted gear is contributed by the bending, shear, and axial compressive deformations. Since the profile shift of the gear will change the dedendum circle without affecting the base circle, two cases need to be considered in the calculation.

Case I: The dedendum circle is smaller than the base circle

When the teeth number with modulus 2 is less than 22 or the modification coefficient is less than 0.6, the

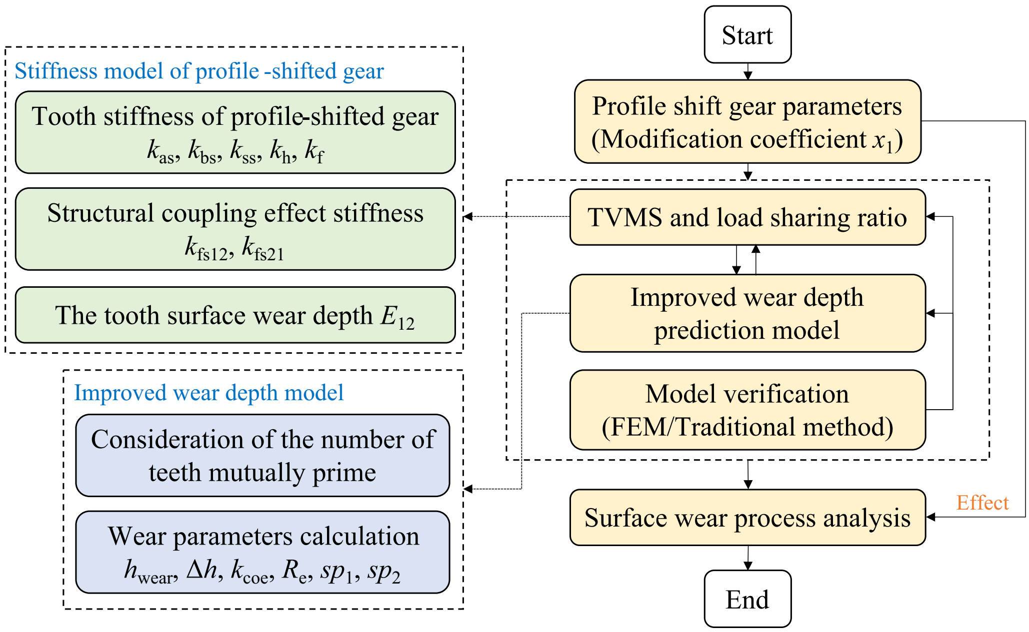

Figure 1 Schematic of this paper

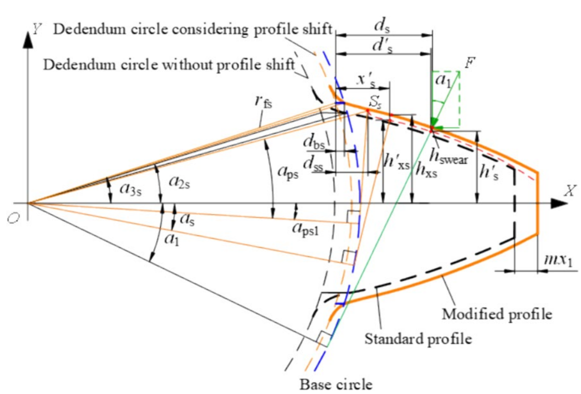

Figure 2 Tooth model of profile-shifted spur gear considering TSW in Case I

dedendum circle is smaller than the base circle as shown in Figure 2. This section takes the tooth of positive profile-shifted gear as the research object with the addendum coefficient h^*a is 1, coefficient of tip clearance c^* is 0.25, pressure angle a_0 is 20 degrees and the modification coefficient is represented by x_1.

Figure 2 shows the comparison of the profile-shifted gear tooth model with TSW and traditional tooth model. The standard profile is represented by the black dotted line and the modified profile is represented by orange line. The tooth profile starts from the dedendum circle and ends at the addendum circle, where tooth wear occurs on the part between base circle and addendum circle which is indicated by the red dotted line. While the transition curve is from the dedendum circle to base circle which is simplified by a straight line [27] and the rest part is the involute curve.

It can be found in Figure 2 that the involute profile of tooth varies with the modification coefficient x_1 and the related parameters also change compared with traditional tooth model. Where the distance d_{bs} is determined by the dedendum circle radius $r_{fs,}$ and the distance d_{ss} is related to the initial meshing point S_s and the angle on the dedendum circle a_{3s}. The values of h'_s, h_{xs} and h'_{xs} are related to the wear depth h_{swear} and the half tooth angle on the base circle a_{2s}. In view of the profile-shifted tooth model, three corresponding stiffness of positive profile-shifted gear tooth can be described based on the gear tooth geometry.

$$\begin{cases} \dfrac{1}{k_{\mathrm{bs}}} = \displaystyle\int_0^{d_{\mathrm{bs}}} \frac{\left[(d_{\mathrm{s}}' - x_{\mathrm{s}}) \cos\alpha_1 - h_{\mathrm{s}}' \sin\alpha_1\right]^2}{EI_{xs}} \mathrm{d}x_{\mathrm{s}}, \\ \quad + \displaystyle\int_{d_{\mathrm{bs}}}^{d_{\mathrm{ss}}} \frac{\left[(d_{\mathrm{s}}' - x_{\mathrm{s}}) \cos\alpha_1 - h_{\mathrm{s}}' \sin\alpha_1\right]^2}{EI_{xs}} \mathrm{d}x_{\mathrm{s}}, \\ \quad + \displaystyle\int_{d_{\mathrm{ss}}}^{d_{\mathrm{s}}'} \frac{\left[(d_{\mathrm{s}}' - x_{\mathrm{s}}') \cos\alpha_1 - h_{\mathrm{s}}' \sin\alpha_1\right]^2}{EI_{xs}'} \mathrm{d}x_{\mathrm{s}}', \\ \dfrac{1}{k_{\mathrm{ss}}} = \displaystyle\int_0^{d_{\mathrm{bs}}} \frac{1.2\cos^2\alpha_1}{GA_{xs}} \mathrm{d}x_{\mathrm{s}} + \int_{d_{\mathrm{bs}}}^{d_{\mathrm{ss}}} \frac{1.2\cos^2\alpha_1}{GA_{xs}} \mathrm{d}x_{\mathrm{s}} + \int_{d_{\mathrm{ss}}}^{d_{\mathrm{s}}'} \frac{1.2\cos^2\alpha_1}{GA_{xs}'} \mathrm{d}x_{\mathrm{s}}', \\ \dfrac{1}{k_{\mathrm{as}}} = \displaystyle\int_0^{d_{\mathrm{bs}}} \frac{\sin^2\alpha_1}{EA_{xs}} \mathrm{d}x_{\mathrm{s}} + \int_{d_{\mathrm{bs}}}^{d_{\mathrm{ss}}} \frac{\sin^2\alpha_1}{EA_{xs}} \mathrm{d}x_{\mathrm{s}} + \int_{d_{\mathrm{ss}}}^{d_{\mathrm{s}}'} \frac{\sin^2\alpha_1}{EA_{xs}'} \mathrm{d}x_{\mathrm{s}}', \end{cases} \tag{1}$$

where k_{bs}, k_{as} and k_{ss} are bending, axial and shear stiffness of profile-shifted gear respectively. The subscript 's' indicates the variables with profile shift and the superscript '′' indicates the variables with TSW respectively. E and G represent modulus of elasticity and rigidity, respectively. I_{xs} and A_{xs} represent the area moment of inertia and the area of the section that has a distance x'_{s} away from the acting point of the applied force F along the profile-shifted gear tooth center line. The main variables in Eq. (1) d_{bs}, d_{ss}, d'_{s}, h_{xs}, h'_{xs} and h'_{s} can be written as:

$$d_{\mathrm{bs}} = 0.5m(2.5 - 2x_1), \tag{2}$$

$$d_{\mathrm{ss}} = r_{\mathrm{b}} a_{\mathrm{ps}} \sin a_{\mathrm{ps1}} + r_{\mathrm{b}} \cos a_{\mathrm{ps1}} - r_{\mathrm{fs}} \cos a_{3s}, \tag{3}$$

$$d'_{\mathrm{s}} = r_{\mathrm{b}}(a_{2s} - a_1) \sin a_1 + r_{\mathrm{b}} \cos a_1 - r_{\mathrm{fs}} \cos a_{3s} - h_{\mathrm{swear}} \sin a_1, \tag{4}$$

$$h_{xs} = \begin{cases} |r_{\mathrm{b}} \sin a_{2s}| \quad \text{if } 0 \le x \le d_{\mathrm{bs}}, \\ r_{\mathrm{b}}(a_{2s} - a_{\mathrm{s}}) \cos a_{\mathrm{s}} - r_{\mathrm{b}} \sin a_{\mathrm{s}}, \quad \text{if } d_{\mathrm{bs}} \le x \le d'_{\mathrm{s}}, \end{cases} \tag{5}$$

$$h'_{\mathrm{xs}} = r_{\mathrm{b}}(a_{2s} - a_{\mathrm{s}}) \cos a_{\mathrm{s}} - r_{\mathrm{b}} \sin a_{\mathrm{s}} - h_{\mathrm{swear}} \cos a_{\mathrm{s}}, \tag{6}$$

$$h'_{\mathrm{s}} = r_{\mathrm{b}}(a_{2s} - a_1) \cos a_1 - r_{\mathrm{b}} \sin a_1 - h_{\mathrm{swear}} \cos a_1. \tag{7}$$

The detail derivation and comparison of above main parameters a_{2s}, a_{3s}, a_{ps}, r_{fs}, x'_{s}, I'_{xs} and A'_{xs} are shown in Appendix A.

Case II: The base circle is smaller than the dedendum circle

When the teeth number with modulus 2 is more than 22 or the modification coefficient is more than 0.6, the base circle is smaller than the dedendum circle as shown in Figure 3. The profile is involute curve between the dedendum circle and the base circle which will be extended by profile shift.

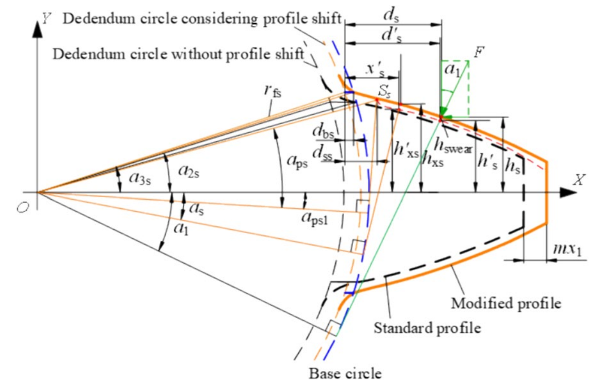

Figure 3 Tooth model of profile-shifted spur gear considering TSW in Case II

Similarly, three corresponding stiffness can be described based on the gear tooth geometry.

$$\begin{cases} \dfrac{1}{k_{\mathrm{bs}}} = \displaystyle\int_0^{d_{\mathrm{ss}}} \frac{\left[(d' - x) \cos\alpha_1 - h_{\mathrm{s}}' \sin\alpha_1\right]^2}{EI_{\mathrm{xs}}} \mathrm{d}x, \\ \quad + \displaystyle\int_{d_{\mathrm{ss}}}^{d_{\mathrm{s}}'} \frac{\left[(d' - x') \cos\alpha_1 - h_{\mathrm{s}}' \sin\alpha_1\right]^2}{EI_{\mathrm{xs}}'} \mathrm{d}x_{\mathrm{s}}', \\ \dfrac{1}{k_{\mathrm{ss}}} = \displaystyle\int_0^{d_{\mathrm{ss}}} \frac{1.2\cos^2\alpha_1}{GA_{\mathrm{xs}}} \mathrm{d}x + \int_{d_{\mathrm{ss}}}^{d_{\mathrm{s}}'} \frac{1.2\cos^2\alpha_1}{GA_{\mathrm{xs}}'} \mathrm{d}x_{\mathrm{s}}', \\ \dfrac{1}{k_{\mathrm{as}}} = \displaystyle\int_0^{d_{\mathrm{ss}}} \frac{\sin^2\alpha_1}{EA_{\mathrm{xs}}} \mathrm{d}x + \int_{d_{\mathrm{ss}}}^{d_{\mathrm{s}}'} \frac{\sin^2\alpha_1}{EA_{\mathrm{xs}}'} \mathrm{d}x_{\mathrm{s}}', \end{cases} \tag{8}$$

where the distance d_{ss} and h_{xs} can be expressed as

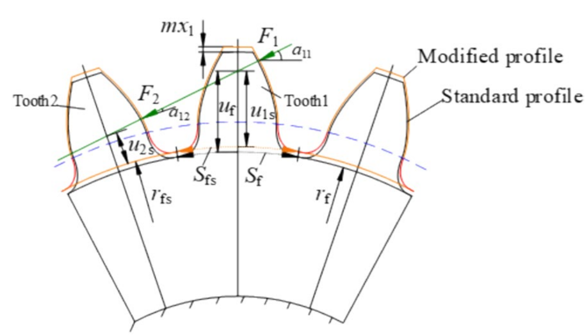

Figure 4 Profile-shifted gear tooth deformation due to structure coupling effect

$$d_{ss}=r_b a_{ps}\sin a_{ps2}+r_b\cos a_{ps2}-r_{fs}\cos a_{5s}, \tag{9}$$

$$h_{xs}=r_b(a_{4s}-a_s)\cos a_s-r_b\sin a_s. \tag{10}$$

Under the action of applied force F, the nonlinear contact Hertzian stiffness has proven by many author [28], which can be calculated using equivalent elastic modulus E_{eq}, width of tooth L, contact force F_i.

$$k_h=\frac{E_{eq}^{0.9}L^{0.8}(F_i)^{0.1}}{1.275}\ F_i=F\times LSR. \tag{11}$$

What is worth nothing is that the load sharing ratio of the profile-shifted meshing tooth pair is *LSR* which is different from standard gear. Thus, the *LSR* will be calculated specially in the following sections. Besides, fillet foundation stiffness can be expressed as

$$k_{fs}=\frac{\cos a_s}{EL}\left[L*\left(\frac{u_{fs}}{S_{fs}}\right)^2+M*\left(\frac{u_{fs}}{S_{fs}}\right)+P*\left(1+Q*\tan^2 a_s\right)\right], \tag{12}$$

where the main parameters u_{fs} and S_{fs} are described in Section 2.2.1 and the symbols L^*, M^* and P^* are given in Ref. [30].

2.2 Mesh Stiffness Calculation Considering TSW Depth and Structure Coupling Effect

2.2.1 Structural Coupling Effect Stiffness of Profile-shifted Gear

An interaction caused by the neighbor meshing tooth pair can pass through the gear body to the other loaded gear teeth pair. Therefore, the fillet foundation stiffness during the double tooth meshing period should be revised by considering the structure coupling effect in order to increase the accuracy of wear analysis process. As shown from Figure 4, fillet foundation deflection of tooth is obtained based on the theory of Muskhelishvili [31]. The profile-shifted gear body structure coupling deformation is defined as the displacement along the line of action when the force F_1 and F_2 applied to the tooth 1 and tooth 2. It should be noted that the parameters u_f and S_f of standard gear tooth varies from the modification coefficient x_1 and the u_{fs} and S_{fs} of modified gear tooth can be obtained from Figure 4.

Based on Ref. [13], the stiffness considering structure coupling effect of profile-shifted gear in double mesh period can be calculated as:

$$\begin{aligned}\frac{1}{k_{fs21}}=\frac{\cos a_{11}\cos a_{12}}{EL}\Bigg[&L_1\left(\frac{u_{1s}u_{2s}}{S_{fs}^2}\right)^2\\&+(\tan a_{12}M_1+P_1)\frac{u_{1s}}{S_{fs}}+(R_1+Q_1\tan a_{11})\frac{u_{2s}}{S_{fs}}\\&+(T_1+S_1\tan a_{11})\tan a_{12}+U_1\tan a_{11}+V_1\Bigg],\end{aligned} \tag{13}$$

$$\begin{aligned}\frac{1}{k_{fs12}}=\frac{\cos a_{11}\cos a_{12}}{EL}\Bigg[&L_2\left(\frac{u_{1s}u_{2s}}{S_{fs}^2}\right)^2\\&+(\tan a_{11}M_2+P_2)\frac{u_{2s}}{S_{fs}}+(R_2+Q_2\tan a_{12})\frac{u_{1s}}{S_{fs}}\\&+(T_2+S_2\tan a_{12})\tan a_{11}+U_2\tan a_{12}+V_2\Bigg],\end{aligned} \tag{14}$$

where the symbols L_i, P_i, R_i, S_i and V_i (i=1,2) can be calculated from Eq. (15), and M_i, Q_i, T_i and U_i can be calculated from Eq. (16). The values from A_i to I_i are listed in Ref. [13].

$$\begin{aligned}X_i(h_{fs},\theta_{fs})=&\frac{A_i}{\theta_{fs}^3}+B_i h_{fs}^3+\frac{C_i}{\theta_{fs}^2}+D_i h_{fs}^2\\&+\frac{E_i h_{fs}^2}{\theta_{fs}}+\frac{F_i h_{fs}}{\theta_{fs}}+\frac{G_i h_{fs}}{\theta_{fs}^2}+H_i h_{fs}+I_i,\end{aligned} \tag{15}$$

$$\begin{aligned}X_i(h_{fs},\theta_{fs})=&A_i\theta_{fs}^3+\frac{B_i}{h_{fs}^3}+C_i\theta_{fs}^2+\frac{D_i}{h_{fs}^2}\\&+\frac{E_i\theta_{fs}}{h_{fs}^2}+\frac{F_i\theta_{fs}}{h_{fs}}+\frac{G_i\theta_{fs}^2}{h_{fs}}+\frac{H_i}{h_{fs}}+I_i,\end{aligned} \tag{16}$$

where the symbol h_{fs} can be expressed as r_{fs}/r_b, and the symbol θ_{fs} is equal to the half angle on the dedendum circle a_{3s} and a_{5s} in Figures 2 and 3.

2.2.2 Mesh Stiffness Calculation Considering TSW Depth

As stated in the introduction, tooth surface wear is a process in which material is removed from the tooth surface, leading to deviation of the tooth profile. Consideration of the factors caused by TSW will eventually complicate the interactions among the contact forces of the tooth pairs during the meshing period. This section regards TSW as the excitation for tooth errors at certain mesh positions, which will change the teeth contact force and further affect the process of TSW. When a pair of gears is in a statically balanced state, the total deformation of each tooth pair is equal to the equivalent displacement on the line of action due to the pinion rotation [32], which can be expressed as:

where the force F in contact can be calculated by moment T and the base circle r_b, and the tooth error E_{12} caused by the TSW is expressed as $E_{12}=h_{wearp2}+h_{wearg2}-h_{wearp1}-h_{wearg1}$.

$$\begin{cases} F_1\left(\frac{1}{k_{bsp1}}+\frac{1}{k_{asp1}}+\frac{1}{k_{ssp1}}+\frac{1}{k_{bsg1}}+\frac{1}{k_{asg1}}+\frac{1}{k_{ssg1}}\right)+F_1\left(\frac{1}{k_{fsp1}}+\frac{1}{k_{fsg1}}\right)+F_2\left(\frac{1}{k_{fsp12}}+\frac{1}{k_{fsg12}}\right)+\frac{F_1}{k_h}+h_{wearp1}+h_{wearp2}=\delta_s, \\ F_2\left(\frac{1}{k_{bsp2}}+\frac{1}{k_{asp2}}+\frac{1}{k_{ssp2}}+\frac{1}{k_{bsg2}}+\frac{1}{k_{asg2}}+\frac{1}{k_{ssg2}}\right)+F_2\left(\frac{1}{k_{fsp2}}+\frac{1}{k_{fsg2}}\right)+F_1\left(\frac{1}{k_{fsp21}}+\frac{1}{k_{fsg21}}\right)+\frac{F_2}{k_h}+h_{wearg1}+h_{wearg2}=\delta_s, \\ F_1+F_2=F, \\ F_1\geq 0,\ F_2\geq 0, \end{cases} \tag{17}$$

where the symbols 'p' and 'g' in the subscripts represent the pinion and gear respectively. The numbers '1' and '2' in the subscripts represent the tooth 1 and tooth 2. F_1 and F_2 are the mesh force in Figure 4. The symbol δ_s denotes the loaded static transmission error of the gear pair when the mesh force F applied. The symbols h_{wear1} and h_{wear2} represent the surface wear depth of tooth 1 and tooth 2 respectively, the calculation of h_{wear1} and h_{wear2} will be shown in Section 3.

Since the wear depth of pinion is much more than that of gear in the same meshing time. It is assumed that the TSW occurs in the pinion and the gear is healthy, the mesh stiffness of single tooth pair can be obtained.

$$\frac{1}{k_{i\_wear}}=\frac{1}{k_{bspi\_wear}}+\frac{1}{k_{aspi\_wear}}+\frac{1}{k_{sspi\_wear}}+\frac{1}{k_{bsgi}}+\frac{1}{k_{asgi}}+\frac{1}{k_{ssgi}}+\frac{1}{k_{fspi}}+\frac{1}{k_{fsgi}}+\frac{1}{k_{hi}},\ i=1,2, \tag{18}$$

where k_{i_wear} denotes the stiffness of ith single tooth pair with TSW. The subscript symbol 'wear' indicates the tooth is worn. Finally, the mesh stiffness of profile-shifted gear with TSW and the load sharing ratio can be obtained from Eq. (17).

$$\begin{cases} k_{m1}=\dfrac{k_{1\_wear}+k_2-k_{1\_wear}k_2\left(\frac{1}{k_{fs12}}+\frac{1}{k_{fs21}}\right)}{1+\frac{k_2E_{12}}{F}\left(1-\frac{k_{1\_wear}}{k_{fs12}}\right)-\left(\frac{k_{1\_wear}k_2}{k_{fs12}k_{fs21}}\right)}, \\ k_{m2}=\dfrac{k_1+k_{2\_wear}-k_1k_{2\_wear}\left(\frac{1}{k_{fs12}}+\frac{1}{k_{fs21}}\right)}{1+\frac{k_{2\_wear}E_{12}}{F}\left(1-\frac{k_1}{k_{fs12}}\right)-\left(\frac{k_1k_{2\_wear}}{k_{fs12}k_{fs21}}\right)}, \end{cases} \tag{19}$$

$$\begin{cases} LSR_1=\dfrac{\frac{1}{k_2}-\frac{1}{k_{fs12}}+\frac{E_{12}}{F}}{\frac{1}{k_{1\_wear}}+\frac{1}{k_2}-\frac{1}{k_{fs12}}-\frac{1}{k_{fs21}}}, \\ LSR_2=\dfrac{\frac{1}{k_1}-\frac{1}{k_{fs21}}-\frac{E_{12}}{F}}{\frac{1}{k_1}+\frac{1}{k_{2\_wear}}-\frac{1}{k_{fs12}}-\frac{1}{k_{fs21}}}, \end{cases} \tag{20}$$

Therefore, the values of the wear depth are calculated and analyzed in Section 3.

3 Improved Wear Depth Prediction Method for a Spur Gear

An improved TSW depth prediction model is employed to calculate and analyze the process of wear in this section, which considers the fact that the number of teeth on the pinion and gear is typically chosen to be mutually prime in the actual working process. According to the concept in Ref. [33], the Archard's model and the depth of nth mesh cycle are given the form as follows:

$$\begin{cases} h_{wear}=\int_0^S k_{coe}P\mathrm{d}s, \\ \Delta h_n=k_{coe}P_n sp, \\ h_{wear,\,n}=h_{wear,\,n-1}+\Delta h_{n-1}, \end{cases} \tag{21}$$

where h_{wear} denotes the depth of the TSW and $\Delta h_{wear,\,n}$ denotes the wear depth of nth mesh cycle at the point applied force, k_{coe} denotes the wear coefficient, P denotes the local contact pressure, s denotes the sliding distance and sp denotes the sliding distance at the point applied force, which can be expressed as follows:

$$k_{coe}=\begin{cases} k_0,\ \lambda<0.5, \\ \dfrac{(8-2\lambda)}{7}k_0, 0.5<\lambda<4, \\ 0,\ \lambda>4, \end{cases} \tag{22}$$

where symbol λ can be expressed as h_{min}/R_r, h_{min} is the minimum film thickness, and R_r is the equivalent surface roughness, and k_0 is the wear coefficient in the boundary lubrication region, the detail expression is shown in Ref. [33].

The calculation of the depth h_{wear} of TSW follows the prediction method in Figure 5. The initial surface and gear parameters are first determined. Consideration of the actual working conditions of gears that the number of teeth on the pinion and gear are typically chosen to be mutually prime. Consequently, when wear occurs on

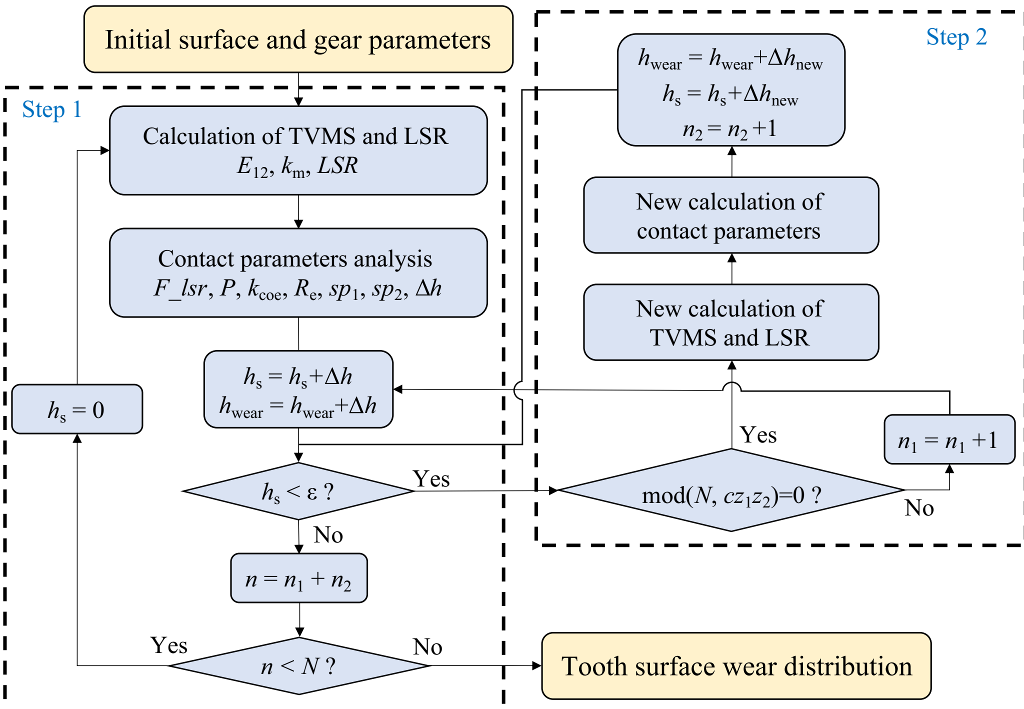

Figure 5 Improved TSW depth prediction method

a tooth of the pinion and a tooth of the gear, the worn tooth surface of the pinion will not continuously engage with the worn tooth surface of the gear. Instead, it will engage with the healthy tooth surface of the gear. The worn tooth surfaces on both the pinion and gear will only come into contact again after $n=z_1z_2$ rotations, where N represents the total number of rotations and z_1 and z_2 represent the number of teeth on the pinion and gear, respectively.

Therefore, the proposed model categorizes the gear TSW process into two distinct steps based on the above characteristics:

Step 1: the pinion with worn surface and the gear with healthy surface

Step 2: the pinion with worn surface and the gear with worn surface

Specifically, when the remainder of the pinion revolution count and z_1z_2 is non-zero, Step 1 is executed, and judge whether the wear threshold ε is reached. Conversely, when the remainder of the pinion revolution count and z_1z_2 is zero, Step 2 is executed, and the TVMS and LSR models are updated accordingly. If the wear threshold ε has not been reached, Step 1 is executed again. The symbol 'c' represents a coefficient to adjust the execution time of Step 2 to simplify the calculation. This partitioning of the wear process facilitates more precise predictions of gear wear. Thus, the main parameter E_{12} of Eqs. (19) and (20) under Step 1 and Step 2 is equal to $-(h_{wearp1}+h_{wearg1})$ and $-h_{wearp1}$ respectively and the wear depth h_{wear} of in Eq. (21) can be expressed as:

$$\Delta h_{wear} = \begin{cases} 2k_{coe}^{s1}P^{s1}a^{s1}\left|\dfrac{u_{g1}^{s1}-u_{p1}^{s1}}{u_{p1}^{s1}}\right|, \text{ Step1,} \\ 2k_{coe}^{s2}P^{s2}a^{s2}\left|u_{g1}^{s2}-u_{p1}^{s2}\right|\left(\dfrac{1}{u_{g1}^{s2}}+\dfrac{1}{u_{p1}^{s2}}\right), \text{Step2,} \end{cases} \tag{23}$$

where the symbols 's1' and 's2' in the superscript represent the step 1 and step 2, respectively, u_{g1} and u_{p1} represent the sliding velocity of the pinion and gear, a is the half Hertzian width. The expression of these

Table 1 The parameters of the gear pair

Parameters		Parameters	
Tooth number	19/48	Modification coefficient	− 0.1~0.4
Modulus (mm)	2	Elastic modulus (Pa)	2.1e11
Pressure angle (°)	20	Poisson's ratio	0.3
Tooth width (mm)	20	Inner bore radius(mm)	10/10
Roughness (μm)	0.3	Input torque (N·m)	300
Rotation speed of pinion speed (r/min)	100	Initial wear coefficient	9.7e−19[34]

parameters can be found in Appendix B. Therefore, the wear depth of pinion can be expressed as follow:

$$h_{\text{wear}} = 2\sum_{i=1}^{n_1} k_{\text{coe},\,i}^{\text{s1}} P_i^{\text{s1}} a_i^{\text{s1}} \left| \frac{u_{\text{g1},\,i}^{\text{s1}} - u_{\text{p1},\,i}^{\text{s1}}}{u_{\text{p1},\,i}^{\text{s1}}} \right| + 2\sum_{j=1}^{n_2} k_{\text{coe},\,j}^{\text{s2}} P_j^{\text{s2}} a_j^{\text{s2}} \left| u_{\text{g1},\,j}^{\text{s2}} - u_{\text{p1},\,j}^{\text{s2}} \right| \left(\frac{1}{u_{\text{g1},\,j}^{\text{s2}}} + \frac{1}{u_{\text{p1},\,j}^{\text{s2}}} \right), \tag{24}$$

where n_1 and n_2 represents the number of Step 1 and Step 2. Thus, the TSW depth h_{wear} can be calculated.

4 Effect of Profile Shift on Wear Process of Spur Gear

4.1 Mesh Stiffness Calculation Considering TSW Depth and Structure Coupling Effect

Verification of the tooth stiffness model with different modification coefficients is given in this section by comparing the results obtained from the FEM. The TSW depth calculated by the improved model is compared with that obtained by the traditional model. The parameters of the gear pair are listed in Table 1.

4.1.1 TVMS and LSR under Different Modification Coefficients

The enhanced model presented in Section 3 is developed using precise calculations of mesh stiffness and load sharing ratio. Using the parameters listed in Table 1, the results of the TVMS and LSR of the standard gear without TSW using three different methods are illustrated in Figure 6. These methods include the traditional method in Ref. [5], the method in this paper, and the FEM. Observing Figure 6, it is evident that the results obtained from the paper method and the FEM demonstrate good agreement for the TVMS and LSR. Conversely, the traditional method, which could not consider the effect of structure coupling, leads to an overestimation of the amplitude of double mesh period stiffness when compared to the paper method in Figure 6(a). Furthermore, the

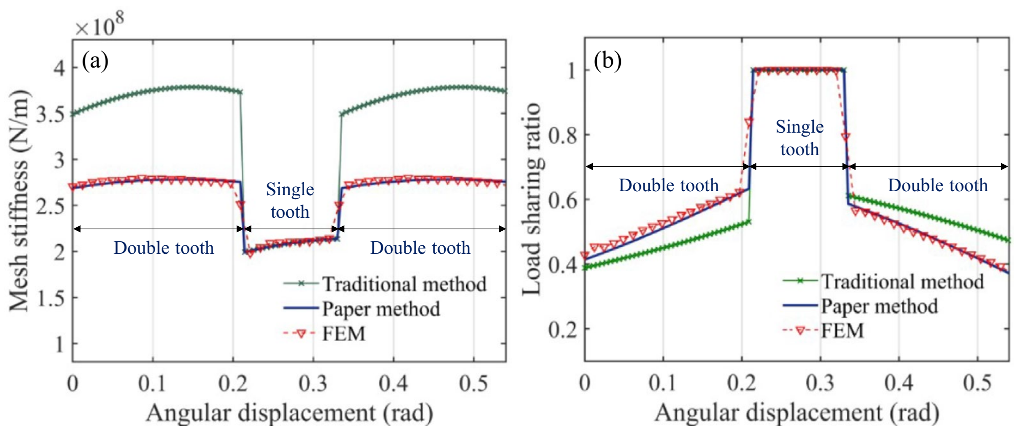

Figure 6 Results of TVMS and LSR of standard gear without TSW using different method: **a** Mesh stiffness in one mesh period, **b** Load sharing ratio in one mesh period

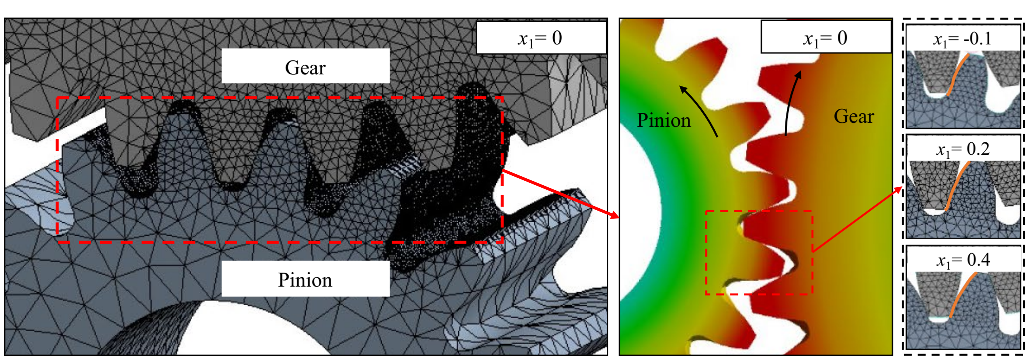

Figure 7 Schematic of finite element model of spur gear with different modification coefficient x_1

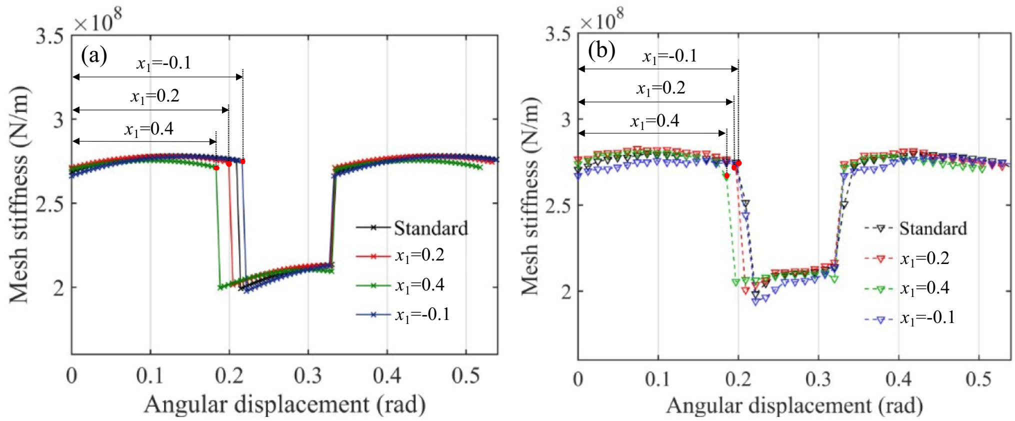

Figure 8 Results of TVMS of profile-shifted gear using different method: **a** Paper method, **b** FEM

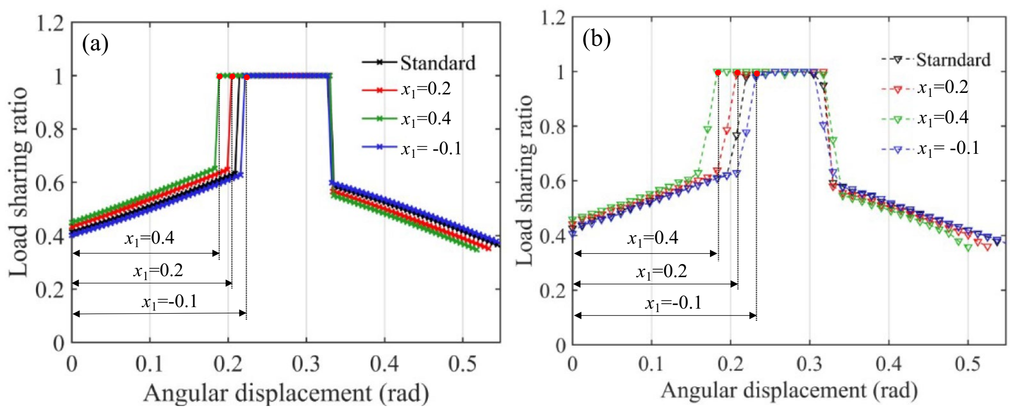

Figure 9 Results of LSR of profile-shifted gear using different method: **a** Paper method, **b** FEM

traditional method yields lower values of LSR during the first double tooth meshing period compared to the paper method, while the former method leads to higher values of LSR during the second double tooth meshing period. This discrepancy is expected to have an impact on the TSW process of gears.

The finite element model is established with different modification coefficient x_1 as illustrated in Figure 7. The torque T is loaded on the gear and the rotation speed N_r is applied to the pinion. Subsequently, the displacement based on the hub bores and tooth pressure force can be obtained and the mesh stiffness and load sharing ratio can be further calculated based on the transient structural module. The results for TVMS and LSR are shown in Figure 6 when the modification coefficient is set to zero. Based on the above descriptions, the TVMS and LSR are analyzed under different modification coefficients. Figures 8 and 9 show the results of TVMS and LSR for the profile-shifted gear without TSW using different method.

It can be found in Figures 8 and 9 that the mesh stiffness and LSR of profiled-shifted gear with modification coefficient x_1 ranging from −0.1 to 0.4 are calculated based on the tooth model. Both methods yielded an error in mesh stiffness and LSR of less than 4%. As x_1 increases from −0.1 to 0.4, the double tooth meshing period gradually decreases from 0.22 to 0.19 rad, while the single tooth meshing period increases from 0.1 to 0.14 rad. And the results in Figures 8 and 9 show the values of the mesh stiffness remain steady, and the LSR of the first double tooth pair increases and decreases in the second double tooth meshing period, which indicates a relationship between the mesh period and modification coefficient x_1. This relationship implies that the tooth surface load in the first double tooth meshing period increases and decreases in the second double tooth meshing period as the x_1 increases. Therefore, the variations in tooth mesh period, the mesh stiffness and the LSR caused by x_1 will further affect the TSW process.

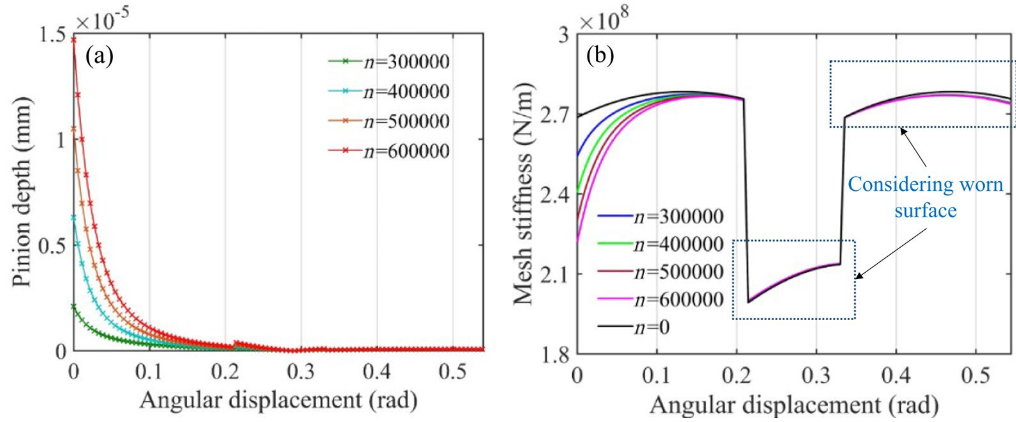

Figure 10 The wear coefficient and TSW depth: **a** The TSW depth of the pinion, **b** The TSW depth of the gear

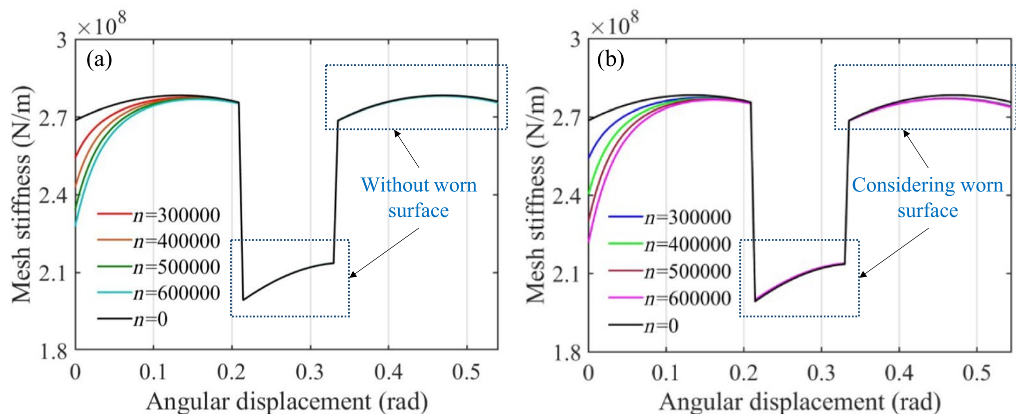

Figure 11 The TVMS of the pinion for Step 1 and Step 2 with different n: **a** Step 1, **b** Step 2

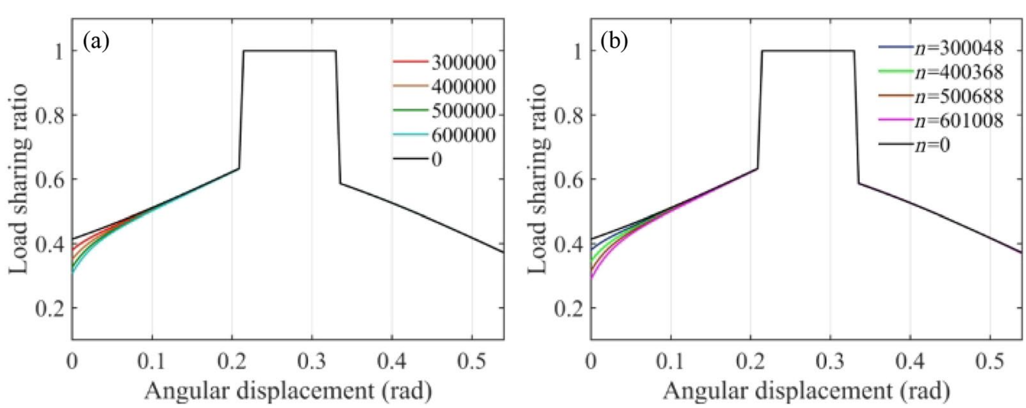

Figure 12 The LSR of the pinion for Step 1 and Step 2 with different n: **a** Step 1, **b** Step 2

4.1.2 TVMS and LSR Considering TSW

In light of the improved wear depth prediction model in Section 3, the analysis of the TSW process is conducted. Figure 10 illustrates the TSW depth for one mesh cycle with varying pinion revolution count n on the basis of Eq. (4). According to Figure 5, n acting on the gear is the number of revolutions that can reach Step 2. As the revolution count n of pinion is considerably higher than that of gear within the same meshing period, the TSW of pinion is more serious than that of the gear. Notably, the severe wear is observed in the tooth root region due to the large contact load, high sliding ratio and large wear coefficient. Since these findings have already been analyzed by Ref. [6] and the phenomenon in this paper align with previous research. Hence, this section does not reiterate the same conclusions.

Unlike previous research, the improved model presented in Section 3 takes into account the primality of the number of teeth, resulting in the TVMS and LSR will be constantly recalculated in Step 1 and Step 2 due to the variations in n. Figures 11 and 12 illustrate the TVMS and LSR for Steps 1 and 2 in Figure 5, respectively, with different revolution counts n. During Step 1, the calculations of TVMS and LSR are based on the worn surface pinion engaging with the healthy surface of the gear. The stiffness values during single tooth meshing period and second double tooth meshing period changes only slightly due to the small wear depth of the pinion as shown in Figure 10(a). During Step 2, the calculations of TVMS and LSR are based on the worn surface pinion engaging with the worn surface of the gear. The stiffness values exhibit a more pronounced variation during single tooth meshing period and second double tooth meshing period. This feature is consistent with the wear depth trends illustrated in Figure 10.

Although there appears to be only a slight change depicted in Figures 11 and 12, it is important to note that this could have a significant impact on the wear depth after numerous iterations and updates, as indicated by our improved model. Figure 13 compares the wear depth (n=600000) of our improved model in this paper with that of a traditional model from Ref. [6]. The

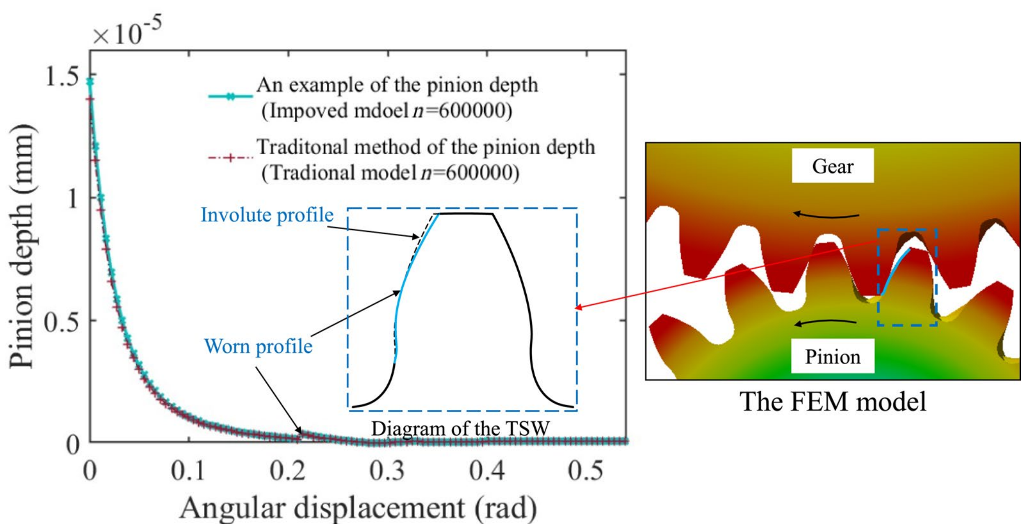

Figure 13 Wear depth comparison and finite element model with TSW (Take the n=600000 as an example)

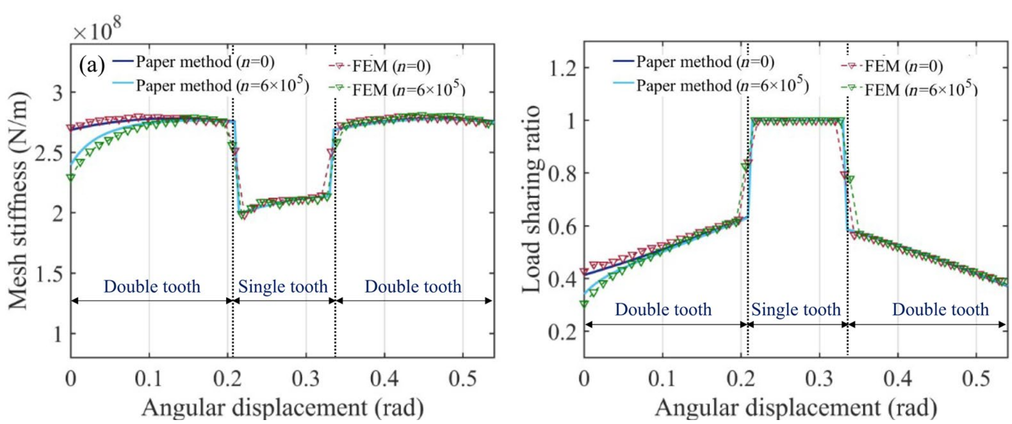

Figure 14 Results of TVMS and LSR of standard gear considering TSW using different method

maximum error occurs at the meshing position of the root of the pinion. The wear depth in this paper method is larger than that obtained by traditional method, with the maximum error is 5%. This finding highlights the significance of the modifications made to our model.

Based on the finite element model, the mesh stiffness calculated by FEM is used to validate the meshing characteristics obtained through paper method. Taking the worn profile of the pinion after 600000 revolution counts as an example, the tooth profile information is imported to establish an irregular tooth profile with TSW as shown in Figure 13.

The mesh stiffness and LSR of standard gear considering TSW are obtained from the two methods as shown in Figure 14. As shown in Figure 14, there has been a sharp drop in TVMS and LSR when the gear pair is engaged, because the maximum of the wear depth is at the tooth root of the pinion. As the TSW gradually decreases, the mesh stiffness returns to normal value. It can be found that the maximum error of the TVMS between the paper method and FEM is about 4% and the variation trend of the paper method is consistent with the FEM. The maximum error may likely be attributable to modeling inaccuracies in Figure 13.

In summary, the variations of the TVMS and LSR caused by the modification coefficient will affect the TSW process. The TVMS and LSR considering the TSW further affect the wear depth as the increase of the revolution count n. Therefore, it is imperative to conduct a more comprehensive analysis of the effect of profile shift on the TSW of spur gears.

4.2 Effect of Profile Shift on TSW of Spur Gear

This section investigates the effect of profile shift on the tooth surface wear (TSW) of spur gears by combining the findings from the previous studies (Sections 2–4.1). The influence of modification coefficient x_1 and revolution count n on the TSW is quantified. Figure 15 presents the

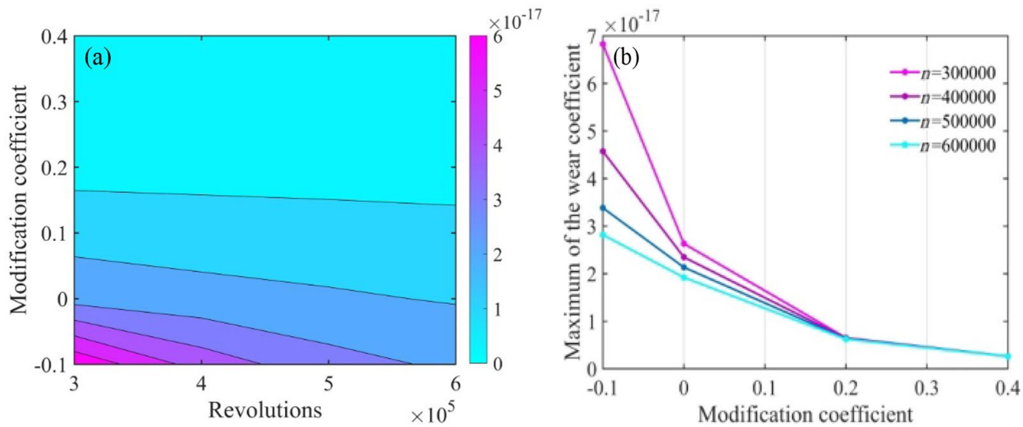

Figure 15 Effect of the modification coefficient x_1 and revolution count n on the wear coefficient k_{coe}: **a** Wear coefficient maximum distribution, **b** The main curve in Figure 15(a)

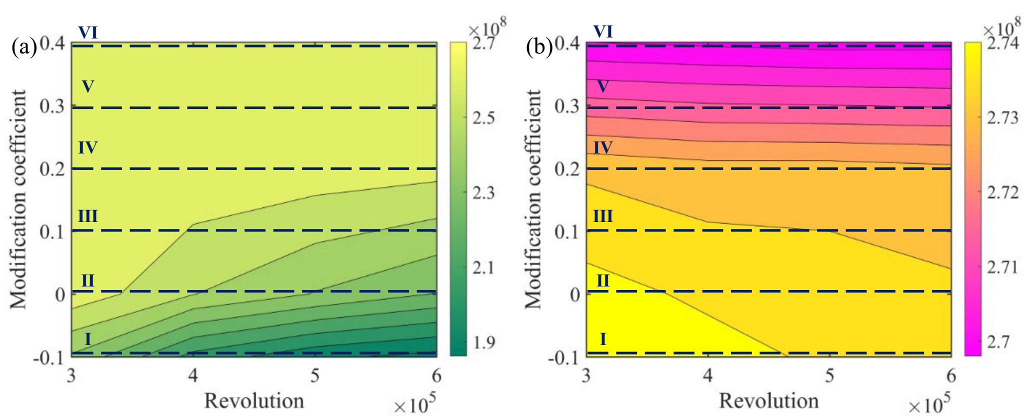

Figure 16 Effect of the modification coefficient x_1 and revolution count n on the mesh stiffness: **a** The distribution of feature values for Step 1, **b** The distribution of feature values for Step 2

effect of the modification coefficient x_1 and revolution count n on the wear coefficient during the meshing process. As shown in Figure 10(a), the maximum of the wear coefficient is a critical parameter. Thus, Figure 15(a) depicts the distribution of the maximum wear coefficient, which reveals that an increase in revolution count and modification coefficient leads to a decrease in wear coefficient, and the value of k_{coe} rises to a peak at 6.9×10^{-17}. Figure 15(b) presents the primary characteristic curve (from I to IV) of wear coefficient k_{coe} with modification coefficient x_1 at different revolution counts n to describe the trends better, which indicates the wear coefficient k_{coe} gradually decreases and the downward trend gradually slows down with the increase of the modification coefficient x_1.

In the above section, an analysis was conducted on the mesh stiffness for Step 1 and Step 2 with a modification coefficient x_1=0. The feature point of the TVMS for Step 1 and Step 2 corresponds to the initial point during the first double tooth meshing and the last point during the second tooth meshing, respectively. Figure 16 presents the effect of the modification coefficient x_1 and revolution count n on the mesh stiffness according to the main characteristic curve (from I to VI). The results demonstrate that the amplitude (from I to VI) of stiffness variation increases with increasing revolution count as the modification coefficient decreases. This finding shows that a smaller modification coefficient has a greater influence on the degree of wear.

Figure 17 illustrates the effect of the modification coefficient x_1 and revolution count n on the wear depth of pinion and gear. It can be observed in Figure 17(a) that as the modification coefficient x_1 decreases and the revolution counts increases, the TSW depth of the pinion increases, with a peak value of 3.6×10^{-5}mm, which demonstrates that the wear depth of the pinion decreases and the downward trend gradually slows down with the modification coefficient increases under different revolution counts.

Conversely, Figure 17(b) indicates that increasing the modification coefficient x_1 and the revolution counts leads to an increase in the TSW depth of the pinion, with a peak value of 2.4×10^{-7}mm, which shows the wear depth of the pinion increases and the upward trend gradually slows down with the modification coefficient increases under different revolution counts. Overall, this finding suggest that a gear positive shift can weaken the TSW depth, while a negative shift will increase it, for the same revolution counts. However, the variation in wear depth resulting from a positive shift in the pinion is significantly greater than that in the gear. Therefore, appropriate gear profile shift could partially alleviate the negative effects of TSW.

5 Conclusions

This paper presents a tooth stiffness model that accounts for profile shift, TSW, tooth deformation, tooth contact deformation, fillet-foundation deformation and gear body structure coupling effect to calculate the TVMS and LSR efficiently and accurately. The results of the TVMS and LSR under different modification coefficients and TSW are validated by the FEM, with the maximum error is less than 4%.

Additionally, an improved wear depth prediction method is developed, which takes into consideration the mutually prime teeth number and more accurately reflects actual gear meshing conditions. Some key parameters such as wear coefficient and wear depth during meshing process can be obtained. Taking the worn profile of the pinion after 600000 revolution counts as an

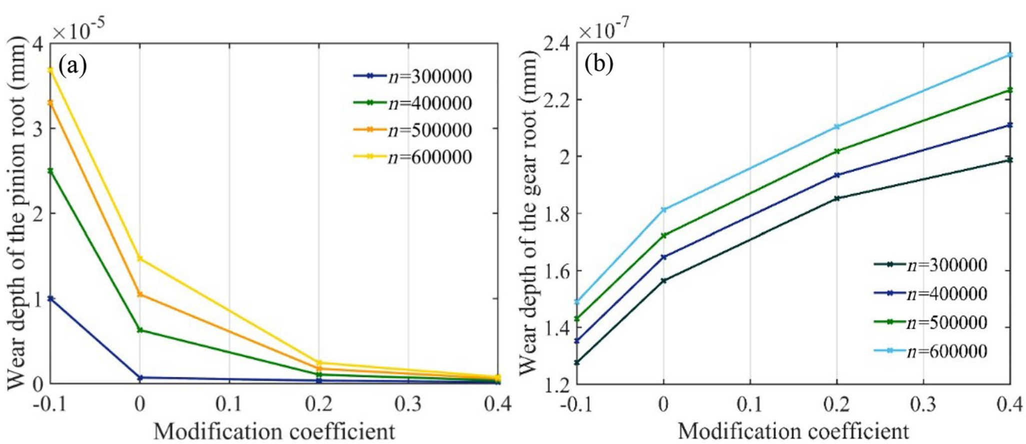

Figure 17 Effect of the modification coefficient x_1 and revolution count n on wear depth: **a** The pinion root wear depth, **b** The gear root wear depth

example, the wear depth in this paper method is larger than that obtained by traditional method, with the maximum error is 5%. Results show that consideration of the mutual prime teeth number will have a certain impact on the TSW process.

The paper also discusses the effect of profile shift on the wear process. On the basis of quantitative analysis, the results show that a positive gear shift can weaken the TSW depth, while a negative shift will increase it, for the same revolution counts. But the variation in wear depth resulting from a positive shift in the pinion is significantly greater than that in the gear. Therefore, an appropriate gear profile shift can partially alleviate the negative effects of TSW.

Appendix A

Figure 18 shows the tooth model with TSW of traditional model. The geometrical relationship of involute profile varies from the modification coefficient x_1. Where r_{fs} denotes the dedendum circle radius of profile-shifted gear, a_{2s} and a_{3s} denote the half angle on the base circle and dedendum, respectively. The main parameters in Figure 2 can be calculated.

$$r_{fs} = r_f + mx_1 = 0.5m(z_1 - 2.5 + 2x_1), \tag{25}$$

$$a_{2s} = \frac{4x_1 \tan a_0 + \pi}{2z_1} + \tan a_0 - a_0, \tag{26}$$

$$a_{3s} = \arcsin\left(\frac{r_b \sin a_{2s}}{r_{fs}}\right). \tag{27}$$

The initial meshing point S varies with the modification coefficient. The value of d_{bs} denotes the distance

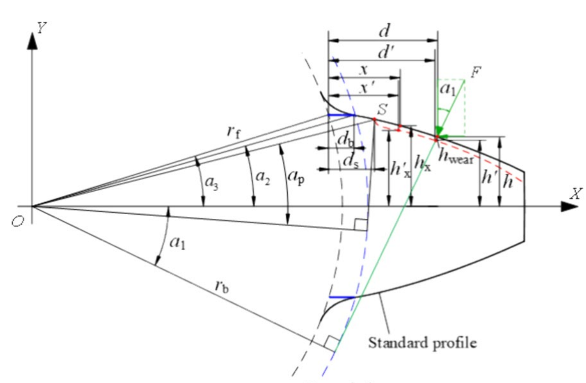

Figure 18 Tooth model with TSW in Ref [5].

from the dedendum circle to the base circle which is equal to d_b-mx_1. The value of d_{ss} denotes the distance from the initial meshing point S_s of profile-shifted gear to the dedendum circle. Then, the variables d_{ss} can be expressed as:

$$d_{ss} = r_b a_{ps} \sin a_{ps1} + r_b \cos a_{ps1} - r_{fs} \cos a_{3s}. \tag{28}$$

Further, the initial meshing angle a_{ps1} and pressure angle a_{ps} on the point S_s can be calculated based on cosine law. Thus, compared with Figure 18 the distance x'_s can be expressed as:

$$\begin{aligned} x'_s = & r_b \cos a_s + [r_b(a_{2s} - a_s) - r_b h_{wear}] \sin a_s \\ & - r_{fs} \cos a_{3s} - mx_1. \end{aligned} \tag{29}$$

Acknowledgements
Not applicable.

Author contributions
WL wrote the manuscript; RZ provided financial support; WZ and JW collated the references. All authors read and approved the final manuscript.

Funding
Supported by National Natural Science Foundation of China (Grant No. 52275061).

Declarations

Competing Interests
The authors declare no competing financial interests.

Received: 29 June 2023 Revised: 21 June 2024 Accepted: 24 June 2024
Published online: 22 July 2024

References

[1] X Z Liu. Vibration modelling and fault evolution symptom analysis of a planetary gear train for sun gear wear status assessment. *Mechanical Systems and Signal Processing*, 2022, 166: 108403.
[2] Y T Sun, Y C Li, Q Zhang, et al. Wear analysis and simulation of small module gear based on Archard model. *Engineering Failure Analysis*, 2023,144: 106990.
[3] K Feng, J C Ji, Y Li, et al. A novel cyclic-correntropy based indicator for gear wear monitoring. *Tribology International*, 2022, 171: 107528.
[4] D. Miler, L Antonio, Ž Dragan, et al. Influence of profile shift on the spur gear pair optimization. *Mechanism and Machine Theory*, 2017, 117: 189-197.
[5] W Chen, Y L Lei, Y Fu, et al. A study of effects of tooth surface wear on time-varying mesh stiffness of external spur gear considering wear evolution process. *Mechanism and Machine Theory*, 2021, 155: 104055.
[6] Y F Huangfu, K K Chen, H Ma, et al. Investigation on meshing and dynamic characteristics of spur gears with tip relief under wear fault. *Technological Sciences*, 2019, 62(11): 1948-1960.
[7] J H Wang, J W Yang, Y L Lin, et al. Analytical investigation of profile shifts on the mesh stiffness and dynamic characteristics of spur gears. *Mechanism and Machine Theory*, 2022, 167: 104529.
[8] H Ma, X Pang, R J Feng, et al. Evaluation of optimum profile modification curves of profile shifted spur gears based on vibration responses. *Mechanical Systems and Signal Processing*, 2016, 70: 1131-1149.
[9] V Kumar, A Kumar, S Kumar, et al. TVMS calculation and dynamic analysis of carburized spur gear pair. *Mechanical Systems and Signal Processing*, 2022, 166: 108436.

[10] K K Chen, Y F Huangfu, H Ma, et al. Calculation of mesh stiffness of spur gears considering complex foundation types and crack propagation paths. *Mechanical Systems and Signal Processing*, 2019, 130: 273-292.
[11] Y Yang, J Y Tang, N Q Hu, et al. Research on the time-varying mesh stiffness method and dynamic analysis of cracked spur gear system considering the crack position. *Journal of Sound and Vibration*, 2023, 548: 117505.
[12] C Y Xie, L Hua, X H Han, et al. Analytical formulas for gear body-induced tooth deflections of spur gears considering structure coupling effect. *International Journal of Mechanical Sciences*, 2018, 148: 174-190.
[13] Z G Chen, Z W Zhou, W M Zhai, et al. Improved analytical calculation model of spur gear mesh excitations with tooth profile deviations. *Mechanism and Machine Theory*, 2020, 149: 103838.
[14] Z Y Chen, P F Ji. Research on the variation of mesh stiffness and transmission error for spur gear with tooth profile modification and wear fault. *Engineering Failure Analysis*, 2021, 122: 105184.
[15] J F Archard. Contact and rubbing of flat surfaces. *Journal of Applied Physics*. 1953, 24: 981–988.
[16] X Zhang, J X Zhong, W Li, et al. Nonlinear dynamic analysis of high-speed gear pair with wear fault and tooth contact temperature for a wind turbine gearbox. *Mechanism and Machine Theory*, 2022, 173: 104840.
[17] H X Tian, H Z Han, Z F Zhao, et al. Wear prediction and meshing characteristics for the planetary gear set considering angular misalignment and rotating carrier. *Engineering Failure Analysis*, 2022, 140: 106583.
[18] Y F Liu, T W Liskiewicz, B D Beake, et al. Dynamic changes of mechanical properties induced by friction in the Archard wear model. *Wear*, 2019, 428: 366-375.
[19] H L Ding, A Kahraman. Interactions between nonlinear spur gear dynamics and surface wear. *Journal of Sound and Vibration*, 2007, 307(3-5): 622-679.
[20] Z X Shen, B J Qiao, L H Yang, et al. Fault mechanism and dynamic modeling of planetary gear with gear wear. *Mechanism and Machine Theory*, 2021, 155: 104098.
[21] K Feng, W A Smith, Z X Peng. Use of an improved vibration-based updating methodology for gear wear prediction. *Engineering Failure Analysis*, 2021, 120: 105066.
[22] H B Wang, C J Zhou, H H Wang, et al. A novel contact model for rough surfaces using piecewise linear interpolation and its application in gear wear. *Wear*, 2021, 476: 203685.
[23] X Z Liu, Y H Yang, J Zhang. Investigation on coupling effects between surface wear and dynamics in a spur gear system. *Tribology International*, 2016, 101: 383-394.
[24] A A Dsa, J Gonsalvis. Effects of altering the tooth-sum on sliding wear of a spur gear. *International Journal of Advanced Research in Engineering*, 2021, 12(1): 669-686.
[25] C J Zhou, X J Dong, H B Wang, et al. Time-varying mesh stiffness model of a modified gear–rack drive with tooth friction and wear. *Journal of the Brazilian Society of Mechanical Sciences and Engineering*, 2022, 44(5): 213.
[26] W Z Liu, R P Zhu, W G Zhou, et al. Probability distribution model of gear time-varying mesh stiffness with random pitting of tooth surface. *Engineering Failure Analysis*, 2021, 130: 105782.
[27] F Liu, Y H Chen, H P Xie, et al. Study on the meshing stiffness of plastic helical gear meshing with metal worm via point-contact. *Mechanism and Machine Theory*, 2022, 176: 105040.
[28] X H Liang, H S Zhang, L B Liu, et al. The influence of tooth pitting on the mesh stiffness of a pair of external spur gears. M*echanism and Machine Theory*, 2016, 106: 1-15.
[29] H Ma, J Zeng, R J Feng, et al. An improved analytical method for mesh stiffness calculation of spur gears with tip relief. *Mechanism and Machine Theory*, 2016, 98: 64-80.
[30] O D Mohammed, M Rantatalo, J O Aidanpää. Dynamic modelling of a one-stage spur gear system and vibration-based tooth crack detection analysis. *Mechanical Systems and Signal Processing*, 2015, 54-55: 293-305.
[31] H B Yang, W K Shi, Z Y Chen, et al. An improved analytical method for mesh stiffness calculation of helical gear pair considering time-varying backlash. *Mechanical Systems and Signal Processing*, 2022: 170.
[32] N I Muskhelishvili. Some basic problems of the mathematical theory of elasticity. *Groningen: Noordhoff*, 1953: 15.
[33] Z G Chen, J Y Wang, K Y Wang, et al. An improved dynamic model of spur gear transmission considering coupling effect between gear neighboring teeth. *Nonlinear Dynamics*, 2021, 106(1): 339-357.
[34] K Feng, J C Ji, Q Ni, et al. A review of vibration-based gear wear monitoring and prediction techniques. *Mechanical Systems and Signal Processing*, 2023, 182: 109605.
[35] V Janakiraman, S Li, A Kahraman. An investigation of the impacts of contact parameters on wear coefficient. *Journal of Tribology*, 2014, 136(3): 031602.

Wenzheng Liu born in 1997, is currently a PhD candidate at *Nanjing University of Aeronautics and Astronautics, China*. His research interests include gear system fault dynamic, signal processing and intelligent monitoring..

Rupeng Zhu born in 1959, a professor and doctoral supervisor at the School of *Nanjing University of Aeronautics and Astronautics, China*. His main research interests include helicopter transmission system, advanced transmission technology and gear dynamic.

Wenguang Zhou born in 1996, is currently a PhD candidate at *Nanjing University of Aeronautics and Astronautics, China*. His main research is the gear elastohydrodynamic lubrication.

Jingjing Wang born in 1989, is currently a PhD candidate at *Nanjing University of Aeronautics and Astronautics, China*. Her main research is the vibration transmission path of helicopter gearbox.